Exact eddy-viscosity equation for turbulent wall flows

Emmanuel Plaut[1] **& Stefan Heinz**[2]
[1]Université de Lorraine, CNRS, LEMTA, F-54000 Nancy, France
[2]Mathematics Department, University of Wyoming, Laramie, WY, USA

Confidential draft **PlautHeinz20.pdf** - Version 0.025 of May 7, 2020

Table of contents

What's new in this Version 0.025 of May 7, 2020

- I inserted the answers of Stefan (mail of May 7, 2020) to Q3 and Q4 in the sections 3.3 and 3.4.

Abstract

A recent theory has been developed (Heinz 2018, 2019) for three canonical turbulent wall flows: channel flow, pipe flow and zero-pressure gradient boundary layer, that offers exact analytical formulas for the RANS eddy-viscosity. By calculating the eddy-viscosity turbulent diffusion term for these flows where the turbulence is stationary, one identifies a high-Reynolds number RANS eddy-viscosity equation with one production and two dissipation terms. One dissipation term is universal and peaks in the near-wall region. The second one is flow-dependent and peaks in the wake region. The production term is flow-dependent and peaks in between. The universal dissipation term implies a damping function and a length scale analogous to the von Karman length scale used in the Scale-Adaptative Simulation models. This length scale also appears in the production term. This confirms on very firm theoretical bases the relevance of von Karman length scales. This is also an occasion to analyze these length scales in more details and propose a new version of the eddy-viscosity equation of the Scale-Adaptative Simulation models.

---

1 Introduction

To be written !..

2 Flow cases and state of the art

2.1 Turbulent wall flows

A part of the text below, especially of the first sentences, will probably move to the introduction...

Wall-bounded turbulent flows are ubiquitous in human-made fluid systems, and are also encountered in the nature: the atmospheric boundary layer for instance is the place where we live and where we like to set up buildings, wind turbines, etc. In the infinite family of these flows, one may distinguish three canonical cases: channel flow, pipe flow and the zero-pressure gradient turbulent boundary layer, or 'boundary layer', for the sake of concision. These flows, denoted here 'turbulent wall flows', are somewhat simpler, because the geometry of the fluid domain is simple and highly symmetric, but they still present a good richness of behaviour. We will build an exact eddy-viscosity equation for these three cases, and discuss the possible consequences on other classical models. Before presenting those, let us fix the hypotheses and notations. We consider an incompressible fluid of mass density ρ and kinematic viscosity ν. In wall-bounded turbulent flows in general, locally a cartesian system of coordinates Oxyz is used, such that x points in the streamwise direction, and y measures the distance to the closest wall. To lowest order, the mean flow

$$\mathbf{U} \;=\; U(y,t)\;\mathbf{e}_x \tag{1}$$

where $\mathbf{e}_x$ is the unit vector in the x-direction, t time. A relevant quantity is the mean strain rate

$$S \;=\; \partial U/\partial y\;, \tag{2}$$

which may be evaluated in more general three-dimensional flows from the full strain-rate tensor, see e.g. the equation (20) of Menter (1997). Focusing now onto the canonical turbulent wall flows, the length scale δ is the half-channel height, pipe radius, or 99% boundary layer thickness with respect to channel flow, pipe flow, and boundary layer, respectively. Denoting $u_x\mathbf{e}_x + u_y\mathbf{e}_y + u_z\mathbf{e}_z$ the fluctuating velocity, the RANS eddy viscosity

$$\nu_t = -\langle u_x u_y\rangle / S \tag{3}$$

where the angular brackets denote the Reynolds average. The mean wall shear stress τ_w is used to define the friction velocity $u_\tau = \sqrt{\tau_w/\rho}$. From this are defined wall or inner units, i.e. $y^+ = u_\tau y/\nu$, $U^+ = U/u_\tau$ and

$$S^+ \;=\; \partial U^+/\partial y^+\;. \tag{4}$$

Finally, the friction-velocity Reynolds number $Re_\tau \;=\; \delta^+ \;=\; u_\tau\delta/\nu$.

2.2 RANS models with an eddy-viscosity equation

To be written, by citing at least Nee & Kovasznay (1969); Baldwin & Barth (1990); Spalart & Allmaras (1994); Menter (1997); Yoshizawa *et al.* (2012) *!..*

2.3 The Scale - Adaptive Simulation models

To be written, by citing at least Menter & Egorov (2006, 2010); Egorov *et al.* (2010); Abdol-Hamid (2015) *!..*
Introduce in particular the von Karman length-scale

$$\ell_{vK} \;=\; \kappa\left|\frac{S}{\partial S/\partial y}\right| \tag{5}$$

and κ the von Karman constant *!..*

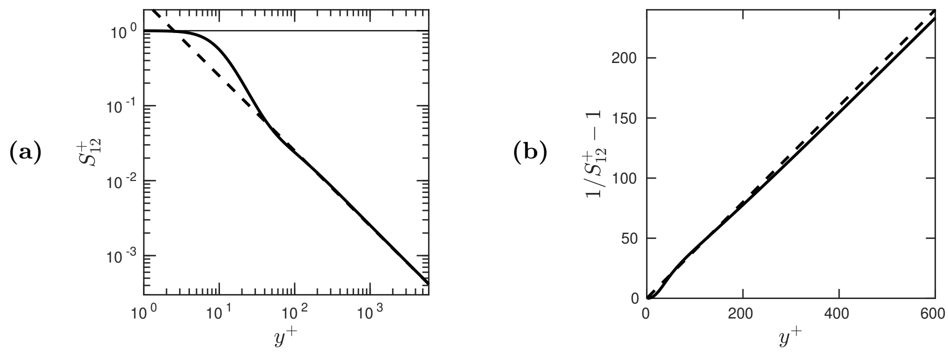

Fig. 1 : **(a)** Continuous line: S_{12}^+ , dashed line: $1/(\kappa y^+)$. **(b)** Continuous line: $1/S_{12}^+ - 1$, dashed line: κy^+.

2.4 Analytic eddy viscosity model of turbulent wall flows

Heinz (2018, 2019) proposed analytic models for the mean flow U, main Reynolds stress $-\langle u_x u_y \rangle$ and eddy viscosity ν_t of the turbulent wall flows defined in section 2.1. In the equation (11) of Heinz (2019), an analytic expression is proposed for the reduced eddy viscosity, which is valid at high Reynolds number, $Re_\tau \gtrsim 500$,

$$\nu^+ \;=\; \nu_t/\nu \;=\; (1/S_{12}^+ - 1)\; N \; . \tag{6}$$

There $S_{12}^+ = S_1^+ + S_2^+$ is a very good approximation of the dimensionless mean strain rate S^+ (4) in the inner region of the flows, i.e., disregarding wake effects, see the equation (7) of Heinz (2018) and the corresponding discussion. Precisely

$$S_{12}^+ \;=\; S_{12}^+(y^+) \;=\; 1 \;-\; \left[\frac{(y^+/a)^{b/c}}{1+(y^+/a)^{b/c}}\right]^c \;+\; \frac{1}{\kappa y^+}\,\frac{1+h_2/(1+y^+/h_1)}{1+y_k/(y^+H)} \;, \tag{7}$$

with

$$a = 9,\quad b = 3.04,\quad c = 1.4,\quad H \;=\; H(y^+) \;=\; (1+h_1/y^+)^{-h_2} \;,\quad h_1 = 12.36,\; h_2 = 6.47,\; y_k = 75.8 \;, \tag{8}$$

and the von Karman constant

$$\kappa \;=\; 0.40 \; . \tag{9}$$

The universal function S_{12}^+ , plotted on the figure 1a, approaches naturally 1 as $y^+ \to 0$ in the viscous sublayer. On the contrary, as $y^+ \to \infty$, $S_{12}^+ \sim 1/(\kappa y^+)$, in agreement with the log law. Therefore the function $1/S_{12}^+ - 1$, plotted on the figure 1b, which appears in the eddy viscosity (6), vanishes in the limit $y^+ \to 0$, and then increases smoothly to approach the function κy^+ as $y^+ \to \infty$.

The second ingredient of the theory is the function N, which is flow-dependent and written in outer scaling, because it describes wake effects. With the notations of Heinz (2018, 2019), $N = 1/G_{CP}$ for channel and pipe flows, M_{BL}/G_{BL} for boundary layers, where G_{CP} and G_{BL} characterize the wake contribution S_3^+ to the dimensionless mean strain rate S^+ (see the equations 7 and A.22 of Heinz 2018), M_{BL} characterizes the total stress in boundary layers (see the equation 4 of Heinz 2019). For channel and pipe flows

$$N \;=\; N_X(y/\delta) \quad \text{with} \quad N_X(y) \;=\; \frac{K_X y + (1-y)^2(0.6y^2+1.1y+1)}{1+y+y^2(1.6+1.8y)} \;, \tag{10}$$

$X = C,\; K_C = 0.933$ for channel, $X = P,\; K_P = 0.687$ for pipe; for boundary layers

$$N \;=\; N_{BL}(y/\delta) \quad \text{with} \quad N_{BL}(y) \;=\; \frac{1+0.285\; y\; e^{y(0.9+y+1.09y^2)}}{1+(0.9+2y+3.27y^2)y} \quad e^{-y^6-1.57y^2} \; . \tag{11}$$

The function N is plotted for these three flows on the figure 2a. In the near-wall region, when $y/\delta \to 0$, $N \to 1$, hence the eddy viscosity (6), $\nu^+ \;=\; (1/S_{12}^+(y^+) - 1)\; N(y^+/\delta^+) \;\sim\; (1/S_{12}^+(y^+) - 1)$ where $\delta^+ = Re_\tau$. Hence the log-layer eddy viscosity κy^+ is approximately recovered if $1 \ll y^+ \ll \delta^+$; for a more precise study, see the section 4.1 of Heinz (2019). When y becomes of the order of δ, wake effects come in, that saturate the growth of the eddy viscosity (6), since N decreases. Whereas the maximum value of y is δ in channel and pipe flows (in channel flow if $y \in [\delta, 2\delta]$ the mean fields can be obtained by suitable symmetries from the mean fields for $y \in [0,\delta]$), it may be much larger in boundary layers. Naturally, $N_{BL} \to 0$ as $y \to \infty$; precisely $N_{BL} < 10^{-3}$ as soon as $y > 1.36\delta$.

The theory of Heinz (2018, 2019) has been validated by a thorough study of DNS data, including those of Lee & Moser (2015); Chin *et al.* (2014); Sillero *et al.* (2013), and experimental data, for instance those of Vallikivi *et al.* (2015). For

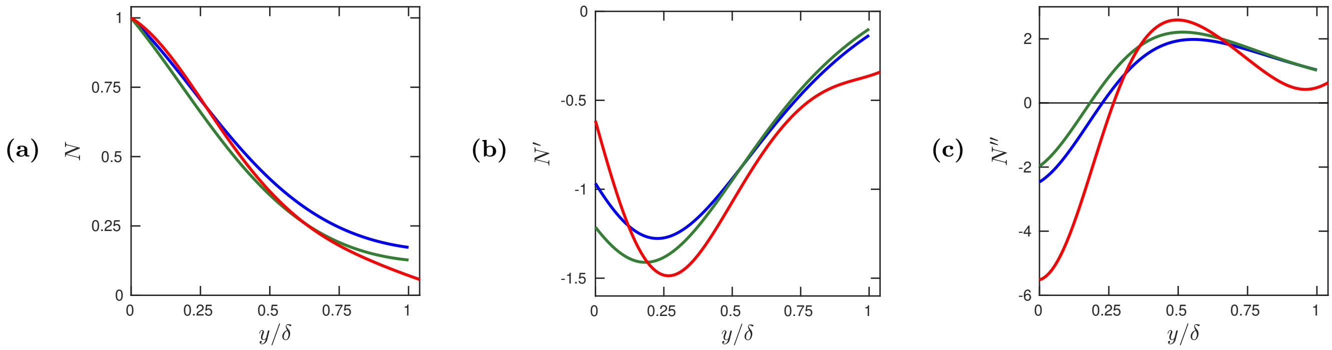

Fig. 2 : **(a)** N **(b)** N' **(c)** N'' for channel (blue), pipe (green), boundary layer (red).

instance, the figures S.6abc of the supplementary material to Heinz (2019) show the eddy viscosity of various DNS, one for each canonical flow, compared with two variants of the eddy-viscosity model (6). In particular, the magenta curves show $\kappa y^+ \ N$ with our notations, i.e. $(1/S_{12}^+ - 1)$ in (6) has been replaced by κy^+. The agreement with the DNS is good, except in the outer region, where in (3) both the numerator $\langle u_x u_y \rangle$ and the denominator dU/dy tend to zero, hence the DNS noise is amplified.
Since the derivatives N' and N'' will be needed hereafer, they are plotted on the figures 2bc. Whereas the functions N for the three flow cases are quite similar (figure 2a), their first and second derivatives show larger differences (figures 2bc).

3 Analysis: exact eddy-viscosity equation

3.1 Generalities

Since the focus of our study is on high-Reynolds numbers wall-bounded flows, we assume that the form of the eddy-viscosity equation is

$$\frac{\partial \nu_t}{\partial t} \ = \ \frac{\partial}{\partial y}\Big(\nu_t \frac{\partial \nu_t}{\partial y}\Big) \ + \ P_\nu \ - \ D_\nu \tag{12}$$

with y the wall distance, $P_\nu > 0$ the production, $D_\nu > 0$ the dissipation term. In the canonical turbulent wall flows, the mean fields are steady, hence the opposite of the turbulent diffusion term

$$-\,T_\nu \ = \ -\,\frac{\partial}{\partial y}\Big(\nu_t \frac{\partial \nu_t}{\partial y}\Big) \ = \ P_\nu \ - \ D_\nu \ . \tag{13}$$

A formal computation of T_ν starting from (6) leads to $D_\nu \ = \ D_{\nu i} \ + \ D_{\nu o}$ and

$$D_{\nu i} \ = \ \kappa^2 \ \frac{\nu_t^2}{L_{vK}^2} \ \frac{1}{f^2} \ , \tag{14a}$$

$$P_\nu \ = \ \kappa \ \frac{\nu_t^2}{L_{vK}\ \delta} \ \frac{1}{1 - S_{12}^+} \ \Big(- \ \frac{4N'}{N} \Big) \ , \tag{14b}$$

$$D_{\nu o} \ = \ \frac{\nu_t^2}{\delta^2} \ \frac{N'^2 + NN''}{N^2} \ . \tag{14c}$$

The indices i and o refer to 'inner' and 'outer' terms, respectively, and the notation $D_{\nu o}$ is slightly improper since this term is slightly negative in the near-wall region. However, it is much smaller in this region than in the outer region where it peaks, as it will be shown in the figures 7ef for channel flow, 8ef for pipe flow, 9ef for boundary layers. In addition to the functions S_{12}^+ and N defined in the section 2.4, there appears in the equations (14) other functions that are built on these. The first one is the asymptotic von Karman length scale

$$L_{vK} \ = \ \kappa \left| \frac{S_{12}}{\partial S_{12}/\partial y} \right| \quad \text{or} \quad L_{vK}^+ \ = \ \kappa \left| \frac{S_{12}^+}{\partial S_{12}^+/\partial y^+} \right| , \tag{15}$$

which is defined as the von Karman length scale ℓ_{vK} (5), but replacing S by S_{12} , i.e., disregarding 'wake effects'. The fact that the length scale L_{vK} appears in (14a) and (14b) confirms on very firm bases the relevance of this length scale, which was not so clear in the works of Rotta. Only the inner-units $L_{vK}^+(y^+)$ is universal, whereas the physical $L_{vK}(y/\delta)$ has to be calculated as $\delta(L_{vK}^+/\delta^+)$, i.e. L_{vK}/δ depends on $\delta^+ = Re_\tau$. Since, as $y^+ \to \infty$, in agreement with the log law, $S_{12}^+ \sim 1/(\kappa y^+)$, $L_{vK}^+ \sim \kappa y^+$, as confirmed by the figure 3a. The functions $\ell_{vK}^+(y^+)$ (figure 3a) or $\ell_{vK}(y/\delta)$

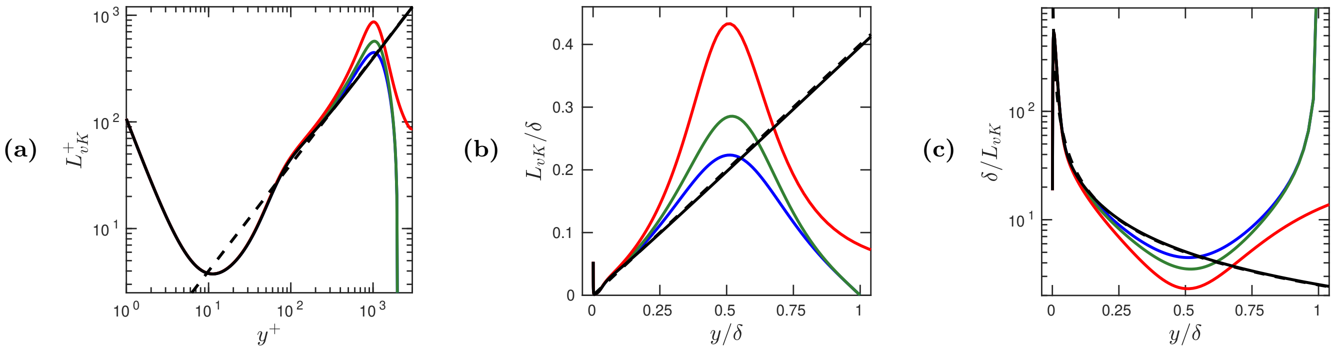

Fig. 3 : **(a,b)** The asymptotic von Karman length scale L_{vK} (15) (black continuous); its log law approximation κy (black dashed); the von Karman length scale ℓ_{vK} (5) for channel (blue), pipe (green), boundary layer (red). The ℓ^+_{vK} curves of the figure **(a)** and all curves of the figure **(b)** have been computed at $Re_\tau = 2000$. All curves have been computed starting at $y^+ = 1$. The figure **(c)** shows the same curves as figure **(b)** but with the inverse ordinates and linear-log scales.

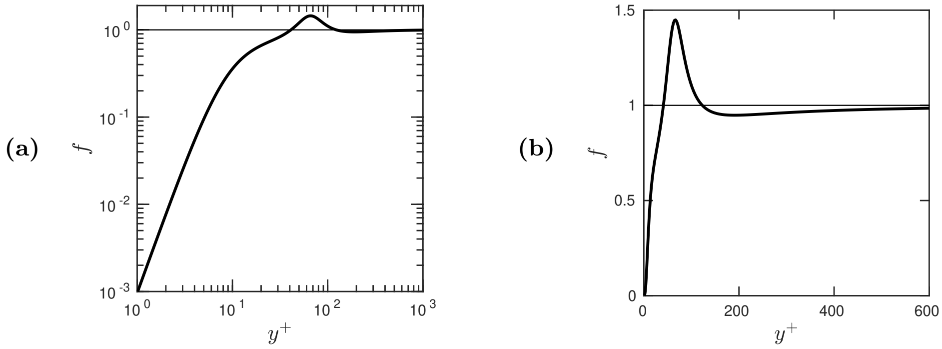

Fig. 4 : The damping function f.

(figure 3b), that depend on the flow case and Reynolds-number, have been computed using the accurate expressions of S^+ of the equation (7) of Heinz (2018). In channel or pipe flow, U presents a maximum at the centerplane or pipe axis $y = \delta$, hence S and ℓ_{vK} vanish there. On the contrary, in boundary layer flow, S and ℓ_{vK} vanish only as $y \to \infty$. The figure 3c suggests that, because the dimensional factor in $D_{\nu i}$ (14a), P_ν (14b) and $D_{\nu o}$ (14c) are respectively ν_t^2/L_{vK}^2 , $\nu_t^2/(L_{vK}\delta)$ and ν_t^2/δ^2, in the ratii δ^2/L_{vK}^2 , δ/L_{vK} , 1, those will peak in the inner, intermediate and outer regions; this will be confirmed in the figures 7 for channel flow, 8 for pipe flow.
Another ingredient in $D_{\nu i}$ (14a), is the universal damping function

$$f \;=\; f(y^+) \;=\; (1 - S^+_{12}) \left(\frac{(S^+_{12} - 1)\; S^+_{12}\; d^2 S^+_{12}/dy^{+2}}{(dS^+_{12}/dy^+)^2} + 3 - 2S^+_{12} \right)^{-1/2} . \tag{16}$$

It is plotted on the figures 4. It does tend to zero as $y^+ \to 0$ and 1 as $y^+ \to \infty$.
Finally, in P_ν (14b) and $D_{\nu o}$ (14c) the rightmost functions depend only on N and its derivatives. These functions are plotted on the figures 5. As already suggested at the level of (13,14), the function $-4N'/N > 0$ everywhere, whereas $(N'^2 + NN'')/N^2 > 0$ except in a more or less narrow near-wall region, depending on the flow case.

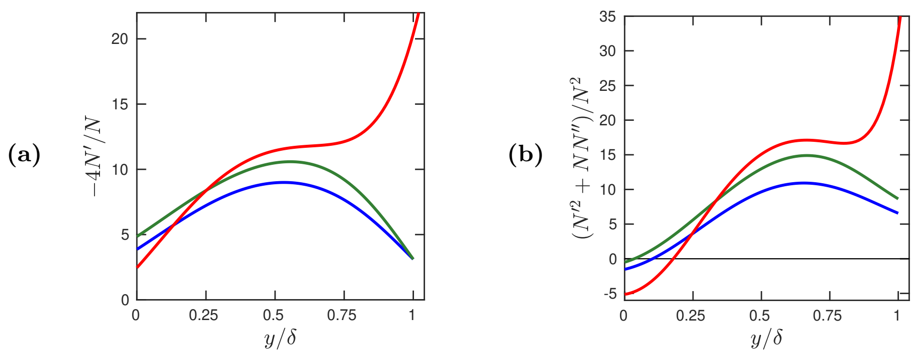

Fig. 5 : For channel (blue), pipe (green), boundary layer (red), the functions $-4N'/N$ in **(a)**, $(N'^2 + NN'')/N^2$ in **(b)**.

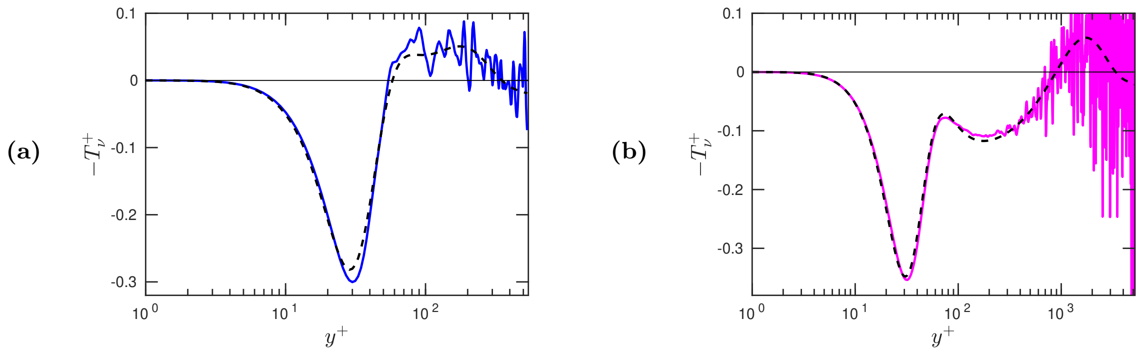

Fig. 6 : The continuous line shows the opposite of the dimensionless turbulent diffusion term $-T_\nu^+$ (17) computed with the channel flow DNS of Lee & Moser (2015) at $Re_\tau = 543$ **(a)**, 5186 **(b)**. The dashed line shows the same term computed with our model (18).

3.2 Application to channel flows

In typical channel flow cases, a comparison of the opposite of the dimensionless turbulent diffusion term

$$-T_\nu^+ \;=\; -\frac{\partial}{\partial y^+}\Big(\nu^+\frac{\partial \nu^+}{\partial y^+}\Big) \tag{17}$$

computed with finite differences from two DNS of Lee & Moser (2015) and its model (13,14),

$$-T_\nu^+ \;=\; P_\nu^+ \;-\; D_\nu^+ \;=\; -\;D_{\nu i}^+ \;+\; P_\nu^+ \;-\; D_{\nu o}^+ \tag{18}$$

is shown on the figures 6. Except in the outer region, where the DNS noise is amplified, there is a good agreement between the model and the DNS, especially, for the highest Reynolds number case.
The separation of $-T_\nu^+$ into the three terms of the model, $-D_{\nu i}^+$, P_ν^+ and $-D_{\nu o}^+$, is illustrated on the figures 7. The comparison of the figures 7a and g shows that the dissipation term $D_{\nu i}^+$ dominates in the near-wall region. In this region, and in inner scalings, $D_{\nu i}^+(y^+)$ approaches as $Re_\tau \to \infty$ a limit profile, that peaks around $y^+ = 31$. Moreover a plateau around $y^+ \simeq 200$ and $D_{\nu i}^+ \;\simeq\; T_\nu^+ \;\simeq\; \kappa^2$ builds up as $Re_\tau \to \infty$, in agreement with the formula for the log-layer reduced eddy viscosity, $\nu^+ = \kappa y^+$. For larger values of y/δ, after this plateau, the figures 7bdfh show that all terms, considered in inner-outer scalings, $D_{\nu i}^+(y/\delta)$, $P_\nu^+(y/\delta)$, $D_{\nu o}^+(y/\delta)$ and $T_\nu^+(y/\delta)$, approach limit profiles as $Re_\tau \to \infty$.

The first 4 values of Re_τ in the figures 7 correspond to DNS of Lee & Moser (2015)*, to allow possible comparisons afterwards: in section 4 I plan a comparison with the SAS models...*

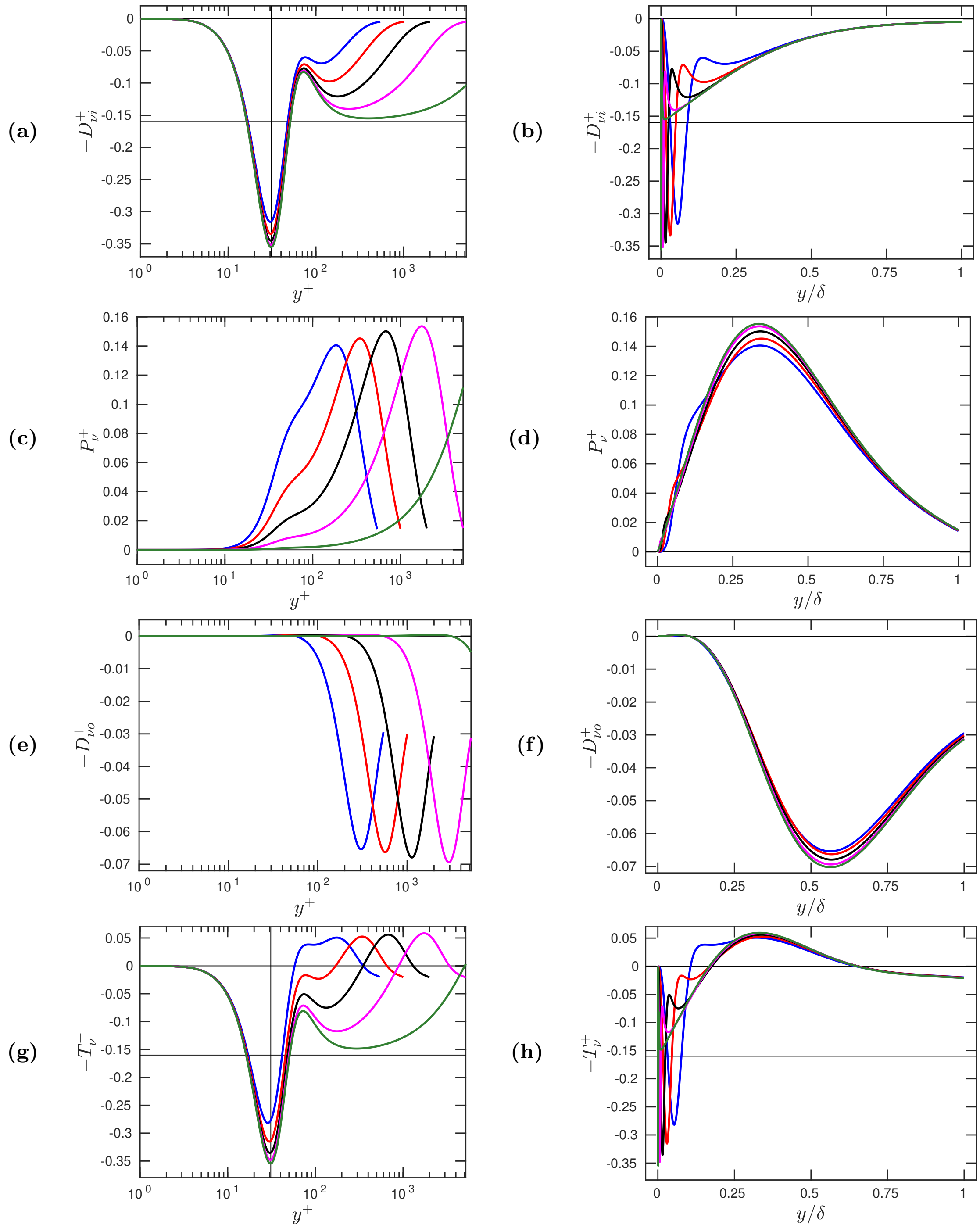

Fig. 7 : For channel flows at $Re_\tau = 543$ (blue), 1001 (red), 1995 (black), 5186 (magenta), 30000 (green), the various contributions to $-T^+_\nu$ (18) and their sum. On **(a,g)** the vertical line is at $y^+ = 31$. On **(a,b,g,h)** the horizontal lines are at $-T^+_\nu = 0$ and $-\kappa^2$.

3.3 Application to pipe flows, with Q3 regarding DNS

- **Q3 :** In order to create a figure similar to the figure 6 but for pipe flows, I would like to get the DNS data of Chin *et al.* (2014).

  Do you think that it would be worthwhile ?

  If yes, should I ask these data to prof. Chin ?

- **R3 : No.**
  This is certainly not worth the effort, and there is no need for that.
  Such plots would be less clear because these data are much more noisy.

In the eddy-viscosity model (6), the only difference between channel and pipe flows is described by the change of the coefficient K_X in the function N_X (10) that contains the wake effects. This change from $K_C = 0.933$ to $K_P = 0.687$ is moderate, therefore the turbulent diffusion term and its contributions are close to the ones of channel flow, as shows the comparison between the figures 7 and figures 8. All the comments made on the figures 7 at the end of section 3.2 also apply to the figures 8.

The first 3 values of Re_τ in the figures 8 correspond to DNS of Chin et al. (2014), to allow possible comparisons afterwards.

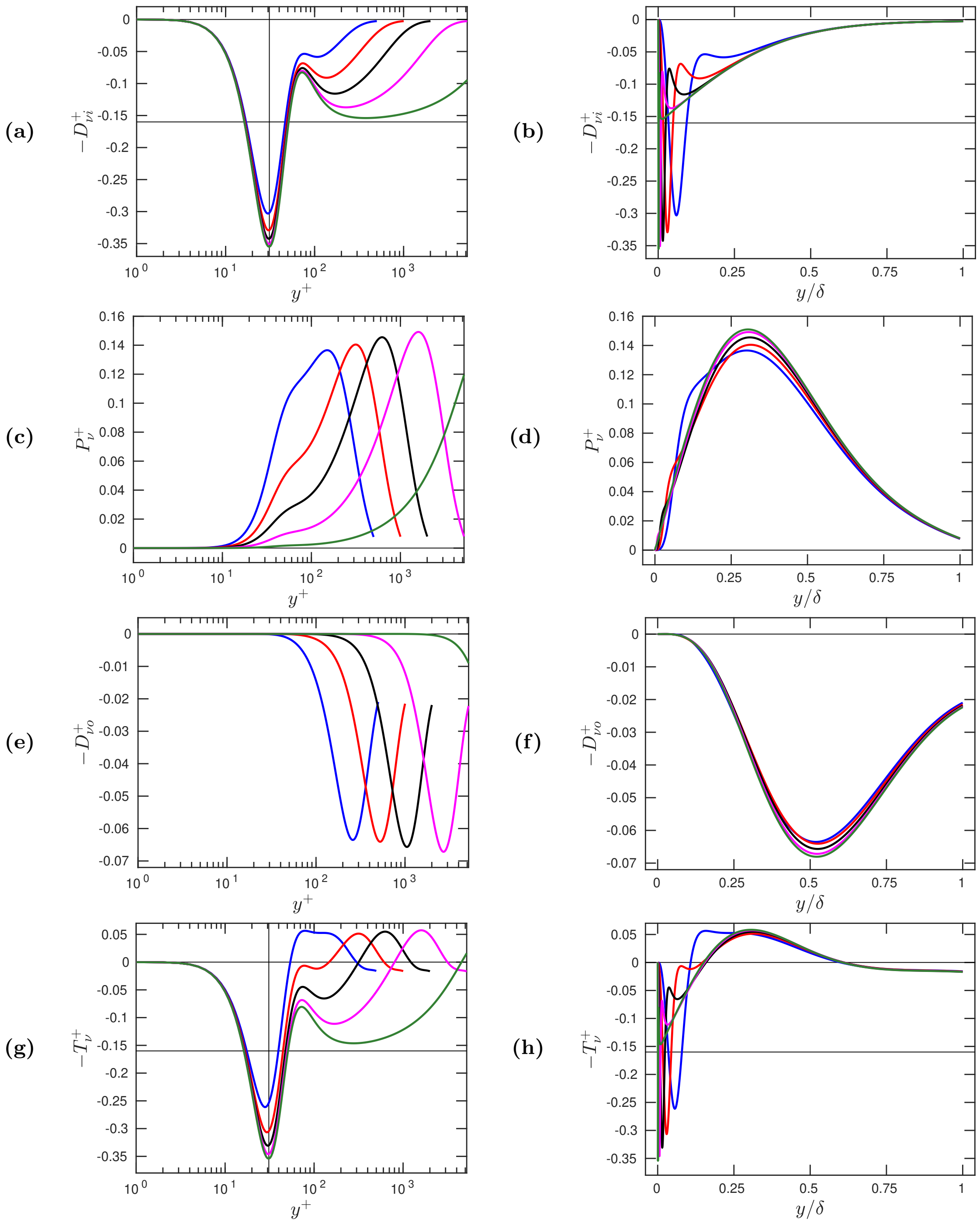

Fig. 8 : For pipe flows at $Re_\tau = 500$ (blue), 1002 (red), 2003 (black), 5186 (magenta), 30000 (green), the various contributions to $-T^+_\nu$ (18) and their sum. On **(a,g)** the vertical line is at $y^+ = 31$. On **(a,b,g,h)** the horizontal lines are at $-T^+_\nu = 0$ and $-\kappa^2$.

3.4 Application to boundary layers, with Q4 regarding DNS

- **Q4 :** I would like to create a figure similar to the figure 6 but for boundary layers, with the DNS data of Sillero *et al.* (2013) - `http://torroja.dmt.upm.es/turbdata/blayers` .

  Do you think that it would be worthwhile ?

- **R4 : No.**
  This is certainly not worth the effort, and there is no need for that.
  Such plots would be less clear because these data are much more noisy.

The boundary layer case differs from the channel and pipe flow cases in that the maximum value of y (resp. y^+) is not δ (resp. $\delta^+ = Re_\tau$) but, in principle infinity. Moreover, the 'wake function' N of boundary layers (11) differs significantly from the one of channel and pipe flows (10). The comparison of the figures 9 with the figures 8 shows similar behaviours in the ranges $y \in [0, \delta[$ i.e. $y^+ \in [0, \delta^+[$, whereas there are slight differences in the outer region. Indeed at $y = \delta$, i.e. the centerplane (resp. pipe axis) for channel (resp. pipe) flow, the function T_ν should present a vanishing slope for symmetry reasons, as confirmed by the figures 7h and 8h. In boundary layers, one does not expect a similar property, but that T_ν should approach 0 as $y \to \infty$. This is what suggests the figure 9h, and what would confirm a figure drawn with a larger interval of the abscissas.

For us only, I created the figures 10, which will be archived and not shown at the end.

The first 3 values of Re_τ in the figures 9 correspond to DNS of Sillero *et al.* (2013)*, to allow possible comparisons afterwards.*

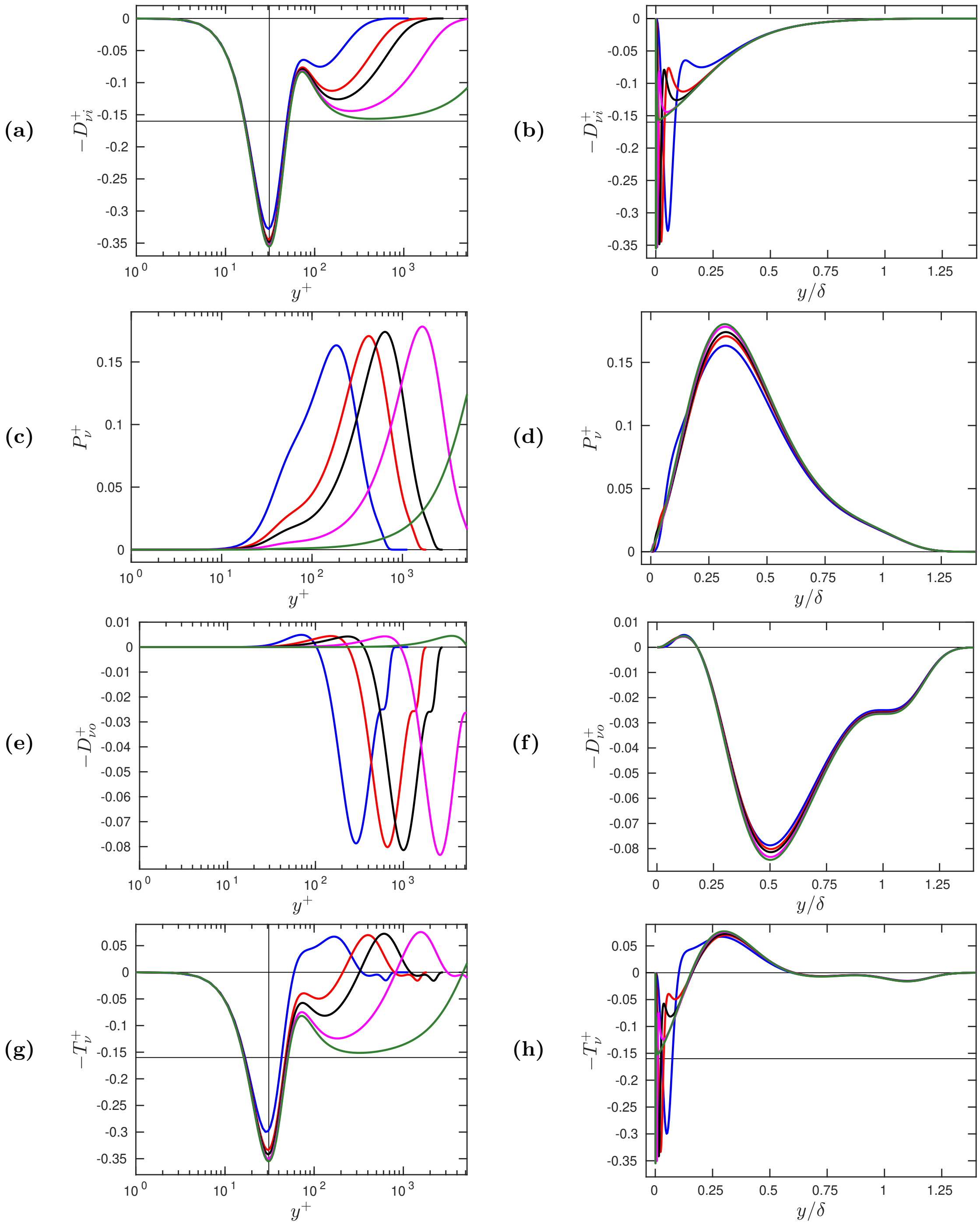

Fig. 9 : For boundary layers at $Re_\tau = 578$ (blue), 1307 (red), 1989 (black), 5186 (magenta), 30000 (green), the various contributions to $-T^+_\nu$ (18) and their sum. On **(a,g)** the vertical line is at $y^+ = 31$. On **(a,b,g,h)** the horizontal lines are at $-T^+_\nu = 0$ and $-\kappa^2$. In all graphs $1 \leq y^+ \leq 1.4\delta^+$.

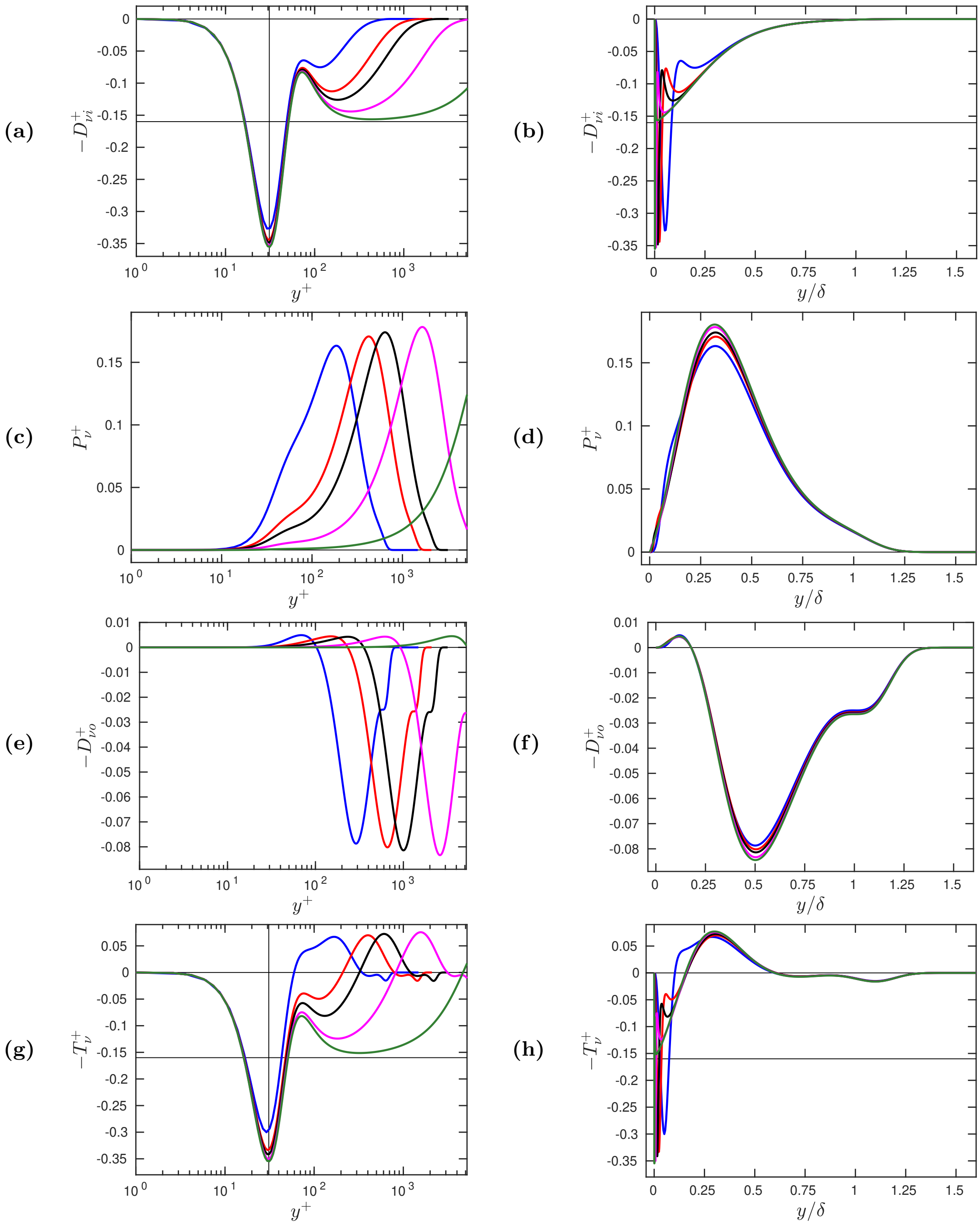

Fig. 10 : Same as figure 9, but in all graphs $1 \leq y^+ \leq 1.6\delta^+$.

4 Discussion

To be written !..

References

ABDOL-HAMID, K. S. 2015 Assessments of $k - kL$ Turbulence Model Based on Menter's Modification to Rotta's Two-Equation Model. *Int. J. Aerospace Engineering* **2015**, 1–18, http://downloads.hindawi.com/journals/ijae/2015/987682.pdf.

BALDWIN, B. & BARTH, T. 1990 A one-equation turbulence transport model for high Reynolds number wall-bounded flows. *NASA Technical Memorandum* pp. 102847, 1–20.

CHIN, C., MONTY, J. & OOI, A. 2014 Reynolds number effects in DNS of pipe flow and comparison with channels and boundary layers. *Int. J. Heat & Fluid Flow* **45**, 33 – 40.

EGOROV, Y., MENTER, F., LECHNER, R. & COKLJAT, D. 2010 The scale-adaptive simulation method for unsteady turbulent flow predictions. Part 2: Application to complex flows. *Flow, Turbulence & Comb.* **85**, 139–165.

HEINZ, S. 2018 On mean flow universality of turbulent wall flows. I. High Reynolds number flow analysis. *J. Turbulence* **19**, 929–958.

HEINZ, S. 2019 On mean flow universality of turbulent wall flows. II. Asymptotic flow analysis. *J. Turbulence* **20**, 174–193.

LEE, M. & MOSER, R. D. 2015 Direct numerical simulation of turbulent channel flow up to $Re_\tau \approx 5200$. *J. Fluid Mech.* **774**, 395–415.

MENTER, F. & EGOROV, Y. 2006 Revisiting the turbulent scale equation. *IUTAM Symposium on One Hundred Years of Boundary Layer Research*, pp. 279–290. Springer.

MENTER, F. R. 1997 Eddy viscosity transport equations and their relation to the $k - \epsilon$ model. *J. Fluids Eng.* **119**, 876–884.

MENTER, F. R. & EGOROV, Y. 2010 The scale-adaptive simulation method for unsteady turbulent flow predictions. Part 1: theory and model description. *Flow, Turbulence & Comb.* **85**, 113–138.

NEE, V. W. & KOVASZNAY, L. S. G. 1969 Simple phenomenological theory of turbulent shear flows. *Phys. Fluids* **12**, 473–484.

SILLERO, J. A., JIMÉNEZ, J. & MOSER, R. D. 2013 One-point statistics for turbulent wall-bounded flows at Reynolds numbers up to $\delta^+ \simeq 2000$. *Phys. Fluids* **25**, 105102,1–16.

SPALART, P. & ALLMARAS, S. 1994 A one-equation turbulence model for aerodynamic flows. *Recherche Aérospatiale* **1**, 5–21.

VALLIKIVI, M., HULTMARK, M. & SMITS, A. J. 2015 Turbulent boundary layer statistics at very high Reynolds number. *J. Fluid Mech.* **779**, 371–389.

YOSHIZAWA, A., ABE, H., MATSUO, Y., FUJIWARA, H. & MIZOBUCHI, Y. 2012 A Reynolds-averaged turbulence modeling approach using three transport equations for the turbulent viscosity, kinetic energy, and dissipation rate. *Phys. Fluids* **24**, 075109.

Archives: link to an important previous version

- **V0.015 of April 29, 2020:** memory of **Q1 & 2** and answers.